Surface Science 672–673 (2018) 68–74

Contents lists available at ScienceDirect

Surface Science

journal homepage: www.elsevier.com/locate/susc

First principles calculations on the influence of solute elements and chlorine adsorption on the anodic corrosion behavior of Mg (0001) surface

Zhe Luo [a], Hong Zhu [b,c,*], Tao Ying [a], Dejiang Li [a], Xiaoqin Zeng [a,*]

[a] National Engineering Research Center of Light Alloys, Shanghai Jiao Tong University, Shanghai 200240, PR China
[b] The State Key Lab of Metal Matrix Composites, Shanghai Jiao Tong University, Shanghai 200240, PR China
[c] University of Michigan - Shanghai Jiao Tong University Joint Institute, Shanghai Jiao Tong University, Shanghai, 200240 PR China

ARTICLE INFO

Keywords:
Mg alloys
Corrosion
First principles calculations
Work function
Local electrode potential shift

ABSTRACT

The influences of solute atoms (Li, Al, Mn, Zn, Fe, Ni, Cu, Y, Zr) and Cl adsorption on the anodic corrosion performance on Mg (0001) surface have been investigated based on first-principles calculations, which might be useful for the design of corrosion-resistant Mg alloys. Work function and local electrode potential shift are chosen as descriptors since they quantify the barrier for charge transfer and anodic stability. We found that at 25% surface doping rate, Y decreased the work function of Mg, while the impact of remaining doping elements on the work function of Mg was trivial due to the small surface dipole moment change. The adsorption of Cl destabilized the Mg atoms at surface by weakening the bonding between surface Mg atoms. We find that a stronger hybridization of *d* orbits of alloying elements (e.g. Zr) with the orbits of Mg can greatly increase the local electrode potential,which even overbalances the negative effect introduced by Cl adsorbates and hence improves the corrosion resistance of Mg alloys.

1. Introduction

As the lightest structural materials with high specific strength, Mg has the potential to be used in auto-mobile industries and aerospace fields [1–3]. However, the poor corrosion resistance of Mg alloys limits their applications [2,4–7], which is believed to related to following factors: 1) magnesium is generally an active metal and the passivation film composed of its oxide and hydroxide is only partially protective [8,9]; 2) small ions like Cl^- in aqueous solutions are believed to be able to penetrate the surface film and accelerate the corrosion [5,10]. Inspired by stainless steels, many efforts have been made to improve the corrosion resistance of Mg by alloying. Unfortunately, Mg matrix is anodic to most secondary phases and trace impurities in the alloy, and the galvanic dipole formed between them will usually accelerate the corrosion [11,12]. Nevertheless, researchers found that alloying may improve the corrosion resistance of Mg by effective grain refinements [13], cathodic kinetics control [14,15], and surface passivation [16]. These findings suggest the practicability of improving the corrosion resistance of Mg by alloying.

Theoretic investigation in Mg corrosion mechanism is indispensable for a better understanding of the corrosion behavior and the design of corrosion-resistant Mg alloys. In the case of pure Mg, Taylor [17] developed a surface reaction kinetic model for hydrogen evolution and anodic dissolution based on first-principles calculations. It has been reported that solute atoms will influence heats of overall hydrolysis reaction of Mg matrix [18] as well as the cathodic behavior of the matrix, such as hydrogen adsorption [19]. In most galvanic corrosion of Mg alloys, the second phases and trace impurities serve as cathodes where hydrogen evolution takes place, while Mg matrix will serve as anode and dissolve in the aqueous solution as ions. Therefore, it is of great significance to study the anodic behavior of Mg matrix, but there were few reports on the impact of solute atoms on the anodic behavior of Mg matrix. Moreover, although the attack of small ions like Cl^- on the Mg surface is implied in various Mg alloys in experiments [5,20,21], there were few theoretical works on how Cl ions accelerate the anode dissolution.

In the anodic reaction, the electrons will transfer from anode to cathode and the atoms on the anode surface will dissolve into the aqueous solution. Work function, which is the minimum work that must be done to remove an electron from the metal [22,23], could describe the degree of difficulty for such a charge transfer. A high work function corresponds to a larger barrier for electrons to escape from a solid and thus better corrosion resistance [24]. Moreover, the corrosion potential is found to be the sum of the potential introduced by work function and contact potential difference at the material and solution interface, so that a positive shift in work function can give rise to a positive shift in corrosion potential [25–27]. On the other hand, the degree of difficulty for an-

* Corresponding author.
E-mail addresses: hong.zhu@sjtu.edu.cn (H. Zhu), xqzeng@sjtu.edu.cn (X. Zeng).

https://doi.org/10.1016/j.susc.2018.02.002
Received 7 November 2017; Accepted 2 February 2018
Available online 16 February 2018
0039-6028/

Table 1
Surface energy and work function of Mg (0001) slabs with 1 × 1, 1 × 2, 2 × 2 surface unit cells.

		Surface energy ($J \cdot m^{-2}$)	Work function (eV)
Surface unit cell	1 × 1	0.55	3.63
	1 × 2	0.56	3.64
	2 × 2	0.53	3.72
Reference		0.54[a], 0.56[b]	3.74[a], 3.66[b]

[a] Computational results from ref [42,43].
[b] Experimental results from ref [44,45].

odic dissolution can be understood as the stability of anode, which can be quantified as the electrode potential. A positive shift in electrode potential implies the stabilization of the electrode[28]. Both experimental observation and first-principles calculations show that solute atoms and adsorbates on the surface are likely to change the work function [29–32] as well as electrode potential [28,33–35].

In this work, first-principles calculations were performed to investigate the influence of Cl adsorbates and solute atoms on the anodic behavior of Mg matrix. Li, Y, Zr, Al, Mn, Fe, Cu and Ni are considered to be solute atoms herein since they are all common alloying or tracing elements in Mg alloys. The work function change and electrode potential shift introduced by the solute atoms and Cl adsorbates were calculated and used to quantify their influence on the anodic behavior of Mg matrix. It is revealed by our calculation that elements like Y at surface will decrease the work function of Mg (0001) surfaces, and elements with strong hybridization with Mg, such as Zr, can raise the local electrode potential and stabilize Mg atoms on the surface.

2. Computational methods

Spin-polarized density functional theory (DFT) calculations were performed by using Vienna ab initio simulation package (VASP) [36] with Perduw–Burke–Ernzerhof functional (PBE) [37] and the projector augmented wave (PAW) [38]. Energy cutoff for plane-wave basis and augmentation charge was 350 eV and Γ-centered *k*-meshes of 14 × 14 × 10 were used for the bulk optimization of Mg primitive cell. The optimized lattice parameters of Mg are: $a = 3.19$ Å, $c = 5.17$ Å, which agree well with the experiment results $a = 3.20$ Å, $c = 5.20$ Å [39]. For doped system, the same energy cutoff 350 eV was applied except Li. For Li-doped slabs, the energy cutoff was 600 eV. In the structural optimization of slabs, the energy convergence criteria were set as 0.1 meV and 1 meV for electronic and ionic relaxations. Methfessel–Paxton scheme [40] was used for *k* space integration during structure optimization. For static calculations, the electronic convergence criterion was 5×10^{-5} meV to get accurate energy, density of states (DOS) and a smooth distribution of charge and electrostatic potential inside materials. Tetrahedron method with Blöchl corrections [41] was adopted for *k* space integration in the static calculations. A slab with 9 monoatomic layers (ML) of Mg atoms with 11 ML of vacuum region (28.5 Å) was good enough to capture the relevant features including work function and surface energy, which are in good agreement with experiments as shown in Table 1.

The electrochemical stability and the corrosion behavior of metals are very sensitive to the surface properties, and surface treatments are usually used to improve the corrosion resistance of metals [46,47]. Anodic dissolution always happens at surfaces and charge transfer also takes place at the surface or interface. Moreover, the enrichment of transition metal elements on Mg surface during corrosion is reported in the experiments [48]. As results, we doped first mono-atomic layer of the Mg (0001) surface to study the influence of solute atoms on the work function and local electrode potential shift.

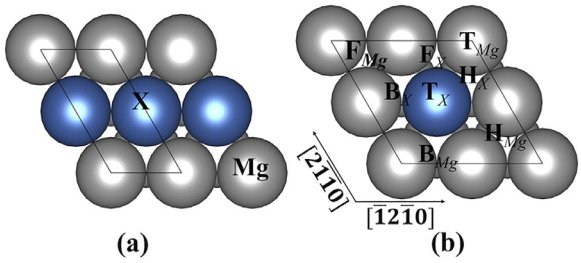

Fig. 1. (a) 50%-doped surface for work function calculation; (b) 25%-doped surface for work function and Cl adsorption calculation; 8 different high-symmetry adsorption sites are considered, including: Mg Top ($\mathbf{T_{Mg}}$), X Top ($\mathbf{T_X}$), Mg-Mg bridge ($\mathbf{B_{Mg}}$), Mg-X Bridge ($\mathbf{B_X}$), FCC hollow all surrounded by Mg atoms ($\mathbf{F_{Mg}}$), HCP hollow surrounded by Mg ($\mathbf{H_{Mg}}$), FCC hollow surrounded by Mg and X ($\mathbf{F_X}$), HCP hollow surrounded by Mg and X ($\mathbf{H_X}$); Mg and dopant are silver and blue spheres and are labelled respectively in (a). (For interpretation of the references to colour in this figure legend, the reader is referred to the web version of this article.)

In work function calculations, two surface doping concentrations, 50% and 25%, were considered here as shown in Fig. 1 (a) and (b). For 50%-doped surfaces, slabs of 2 × 1 surface unit cells were used with a Γ-centered *k*-meshes of 7 × 14 × 1, while for 25%, 2 × 2 surface unit cells with Γ-centered *k*-meshes of 7 × 7 × 1 were adopted. Work function is defined as the energy difference between vacuum level and the Fermi level of the slab as displayed:

$$\phi = \Phi_{vac} - E_{fermi}, \tag{1}$$

where Φ_{vac} is the vacuum level and E_{fermi} is the Fermi level of the slab. The Fermi level is calculated by following steps: first we calculate the difference between the Fermi level and the averaged electrostatic potential in bulk Mg; then we calculate the averaged electrostatic potential within the bulk region in the Mg slab; finally we add the aforementioned difference in bulk to the averaged electrostatic potential in slab to obtain the position of Fermi level in the slab [29].

Local electrode potential shift ΔV introduced by Cl adsorbates on Mg (0001) is labelled as ΔV^{Cl}, while ΔV^{alloy} stands for the ΔV introduced by solute atoms, and $\Delta V^{alloy,\ Cl}$ is the shift due to simultaneously effects of solute atoms and Cl adsorbates. For simplification, superscript A is used to represents the aforementioned 3 factors (Cl adsorption, alloying and both Cl adsorption and alloying together), and the corresponding electrode potential shift is labelled as ΔV^A. To calculate ΔV^A, we started from the local dissolution process of Mg on the surface at initial stage, which is the escapes of a Mg from the surface and generation of a Mg surface vacancy as expressed below:

$$Mg^{pure/A} \rightarrow Mg_{vac}^{pure/A} + Mg^{n+} + ne^-, \tag{2}$$

where $Mg^{pure/A}$ represents the pure Mg slabs and Mg slabs with aforementioned effect A, and $Mg_{vac}^{pure/A}$ is the corresponding slab with a vacancy on the surface; Mg^{n+} represents the dissolved Mg ions from surface; n is the transferred charges during the reaction. Here we assume that the charge transfer remains constant throughout pure system and all alloy systems. The open circuit voltage of the electrode can be calculated with the Gibbs free energy change of the corresponding reaction. With regard to standard hydrogen electrode (SHE), the open circuit voltage of the reaction in Eq. (2) is given by [49]:

$$-neV_{Mg}^{pure/A} = n\mu_{H^+}^0 + G(Mg^{pure/A}) - G(Mg_{vac}^{pure/A}) - G(Mg^{n+}) - n/2\mu_{H_2}^0, \tag{3}$$

where $V_{Mg}^{pure/A}$ stands for the local electrode potential of pure Mg slab or Mg slab with *A; G* standards for the Gibbs free energy of the slab configuration or ions in the brackets; $\mu_{H^+}^0$ and $\mu_{H_2}^0$ are the chemical potential of H^+ and H_2 at standard states. If the concentrations of Mg^{n+} is kept invariant in pure and doped systems, which is often adopted in the experiments, the Gibbs free energies of Mg^{n+} in two reactions

are the same. Moreover, it is safe to assume that the entropy terms in the Gibbs free energy cancelled during the calculations, so that we can replace the Gibbs free energy G with the DFT energy E. As results, the local electrode potential shift introduced by A with regard to pure Mg surface, $\Delta V^A = V^A_{Mg} - V^{pure}_{Mg}$ can be calculated by:

$$ne\Delta V^A = G(Mg^{pure}) - G(Mg^{pure}_{vac}) - (G(Mg^A) - G(Mg^A_{vac})). \quad (4)$$

It is quite close to Ma's methods for PtM_3 alloys [34], where M stands for the alloying elements, whereas we did not apply his approximation of $(E(Mg) - E(Mg_{vac}))$ as the surface chemical potential of Mg. Given the possible existence of unipositive Mg during corrosion process [4,50], the transferred charges n should stay in the range between 1 and 2. Because n is already assumed constant throughout all the cases (pure slab, alloyed slabs, slabs with Cl adsorbate and alloyed slab with Cl adsorbate) and comparison is of more interest between the electrode potential shift introduced by different factors, the exact value of n is not so important. It needs to be emphasized that steps and kinks on the surface or surfaces with different miller index are also likely to change the local electrode potential, which makes the potential in Equation (3) at standard condition differ from the standard hydrogen potential of Mg. But our focus here is the influence of chemical composition, so the surface topography is not covered in our study.

In the calculation of ΔV^A, slabs with 2×2 unit cells are adopted as shown in Fig. 1 (b). It is expected that the pure Mg slabs with Cl adsorbate (Mg^{Cl}) and alloyed Mg slabs with Cl adsorbate ($Mg^{alloy,\,Cl}$) and their corresponding structure with vacancy (Mg^{Cl}_{vac} and $Mg^{A,Cl}_{vac}$) in the reaction expressed by Eq. (2) have different configurations. The most energetic favored configurations are of specific interest here and used in the calculation of local potential shift. For slab with Cl adsorbates, the most stable configuration is one with lowest Cl adsorption energy E^{Cl}_{ads}, which is defined as:

$$E^{Cl}_{ads} = \frac{1}{2}(E(Mg^{Cl,pure/alloy}) - E(Mg^{pure/alloy}) - 2E_{Cl}), \quad (5)$$

where $E(Mg^{Cl,\,pure/A})$, $E(Mg^{pure/A})$ and E_{Cl} represent the DFT energy of pure/alloyed slab with Cl adsorbate, clean pure/alloyed slab and single Cl atom respectively. The factor of 2 in the denominator results from the fact that Cl adsorbates are putted on each side of the slab with symmetry. All the possible adsorption sites for pure Mg surface are considered, including top site, bridge sites, fcc/hcp hollow sites. For doped surfaces, all 8 high-symmetry adsorption sites are also considered as shown in Fig. 1 (b): $\mathbf{T}_{Mg}$,$\mathbf{T}_X$,$\mathbf{B}_{Mg}$, $\mathbf{B}_X$, $\mathbf{F}_{Mg}$, $\mathbf{H}_{Mg}$, $\mathbf{F}_X$, $\mathbf{H}_X$. When the energy difference between certain configuration of Mg^{Cl} or $Mg^{alloy,\,Cl}$ and the most stable one is less than 0.025 eV (~Boltzman constant times room temperature), the corresponding local electrode potential is also calculated and listed in Table S1 for comparison.

3. Results and discussion

3.1. Work function of doped Mg (0001) surface

Work functions of doped Mg (0001) surfaces are displayed in Table 2 and plotted in Fig. 2 with respect to their electronegativity. For 50% doping rate, elements more electronegative than Mg will increase the work function on Mg (0001). When the surface doping concentration decrease from 50% to 25%, the influence of doping elements on the work function is greatly reduced for most cases. Only yttrium has a strong impact at 25% doping rate, severely reducing the work function, which indicates that Y doping will make electrons more easily to escape from the surface compared to pure Mg.

Generally when the surface dopant is more electronegative than Mg, the dopant will be negatively charged and cause a negative dipole on the surface, which will lead to an increase in work function. However, the changes in work function are not just determined by the quantity and the sign of charge transferred between dopants and Mg atoms, but also by the details of the charge redistribution [51]. Work function difference is more related to the charge redistribution perpendicular to the surface. To be more specific, it is reported that the work function difference is linear to the surface dipole moment change [51,52]:

$$\Delta\phi = -4\pi\Delta\mu/A, \quad (6)$$

where $\Delta\mu$ is the surface dipole moment change only dependent on the charge redistribution perpendicular to surface, $\Delta\phi$ is the corresponding work function difference and A is the surface area.

The work function of 25%-doped Mg surface is plotted in Fig. 3 with respect to the surface dipole moment change, which reveals that influence of doping elements here on the surface dipole moment change is also negligible except Y. The small change in surface dipole moment introduced by most dopants here indicates that charge transfer perpendicular to the surface is not strong or the vertical charge displacement is small at 25%-doping concentration. Since the dopants are within surface atoms plane, the charge transfer between dopants and the remaining 3 Mg atoms in the same mono-atomic layer can be mainly parallel to the surface, and the displacement of charge perpendicular to surface might be more obvious if the radius of dopants and Mg are very different. Large decrease introduced by Y may result from the combination of several factors: Yttrium has the greatest atomic radius 1.80 Å [53] among dopants considered here, which allows larger charge displacement perpendicular to the surface than other dopants; Y located at higher position

Table 2
Work function (eV) of 50%-doped and 25%-doped Mg (0001), most stable Cl adsorption site and corresponding Cl adsorption energies (eV) of 25%-doped Mg (0001).

Dopant	Work function		Cl adsorption	
	50%	25%	site	E^{ads}_{Cl}
pure	3.64	3.72	$\mathbf{F}_{Mg}$	−4.156
Li	3.60	3.68	$\mathbf{H}_X$	−4.362
Y	3.18	3.29	$\mathbf{F}_X$	−4.701
Zr	3.63	3.71	$\mathbf{T}_X$	−4.824
Mn	3.82	3.73	$\mathbf{F}_X$	−4.230
Al	3.75	3.74	$\mathbf{F}_{Mg}$	−4.350
Zn	3.72	3.75	$\mathbf{F}_{Mg}$	−4.334
Fe	3.74	3.71	$\mathbf{F}_{Mg}$	−4.249
Cu	3.74	3.71	$\mathbf{F}_{Mg}$	−4.353
Ni	3.72	3.69	$\mathbf{F}_{Mg}$	−4.412

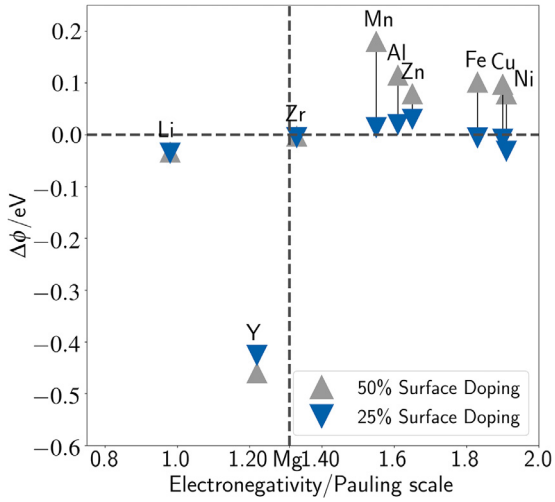

Fig. 2. Work function change of Mg (0001), $\Delta\phi$ in presence of surface doping as a function of electronegativity of dopants. Dashed horizontal and vertical lines represent the work function and electronegativity of Mg respectively.

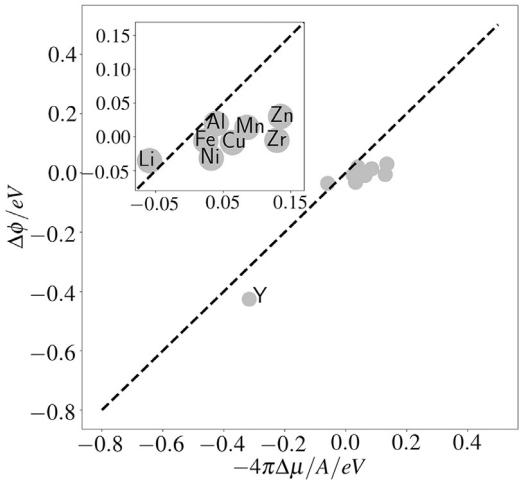

Fig. 3. Work function change $\Delta\phi$ plotted as a function of surface dipole moment difference for $\Delta\mu$ 25% doped Mg (0001) slabs. The dashed line represents the theoretical relation between $\Delta\phi$ and $\Delta\mu$.

Table 3
Cl adsorption energy E_{ads}^{Cl} (eV) on pure Mg (0001) and local electrode potential shift by Cl adsorption with respect to pure clean Mg surface, ΔV^{Cl} (V).

	Adsorption site	This work	Reference
E_{ads}^{Cl}	$\mathbf{T}_{Mg}$	−3.540	−3.557[a]
	$\mathbf{B}_{Mg}$	−4.019	
	$\mathbf{H}_{Mg}$	−4.103	−4.147[a]
	$\mathbf{F}_{Mg}$	−4.111	−4.156[a]
ΔV^{Cl}		−0.099	

[a] Computational results from ref [43].

than the average Mg atoms at surface; Y is less electronegative than Mg hence positively charged. The combination of these factors results in a large positive surface dipole moment compared to other elements, thus leading large decrease in work function.

3.2. Local electrode potential shift

3.2.1. Local electrode potential shift introduced by Cl adsorption on pure Mg (0001)

For pure Mg (0001), the Cl adsorption energy on varied site and the local electrode potential shift introduced by Cl adsorbate with respect to pure clean Mg surface, ΔV^{Cl} are shown in Table 3, where $\mathbf{F}_{Mg}$ is the most stable Cl adsorption sites, similar to the work of Zhou et al. [43]. The bond length of Cl and Mg without doping is 2.57 Å, very close to the sum of ionic radii of Mg and Cl ion, 2.53 Å [53,54]. As mentioned, positive electrode potential shift represent the stabilization of surface Mg atoms. So the negative electrode potential shift, $\Delta V^{Cl} = -0.099$V, implies that Cl adsorbates destabilize Mg atoms on the surface.

To understand the negative local potential shift introduced by Cl, detailed information on the surface chemical environment is necessary. Fig. 4 (d) (e) illustrates the site-projected DOS of Cl, and two types of Mg atoms, Mg^1 atom and Mg^2 atom in Fig. 4 (a) when Cl is on the FCC hollow sites. The highest DOS peaks of both Cl atom and Mg^1 atom lie about -5.1 eV below Fermi level, indicating strong Mg-Cl chemical bonding plotted as orange lines in Fig. 4 (a); the highest DOS peak of Mg^2 atom, lies about -5.3 eV below Fermi level and the amplitude is much smaller, indicating Mg^2 atom is barely involved in the bonding with *Cl*. On pure Mg surface, metallic bonds between Mg atoms need to be broken to remove Mg atoms, which is formed by the attraction between positively charged metal ions and delocalized "free" electrons. Due to the localization of electrons after Cl adsorption, the "free" electrons shared by

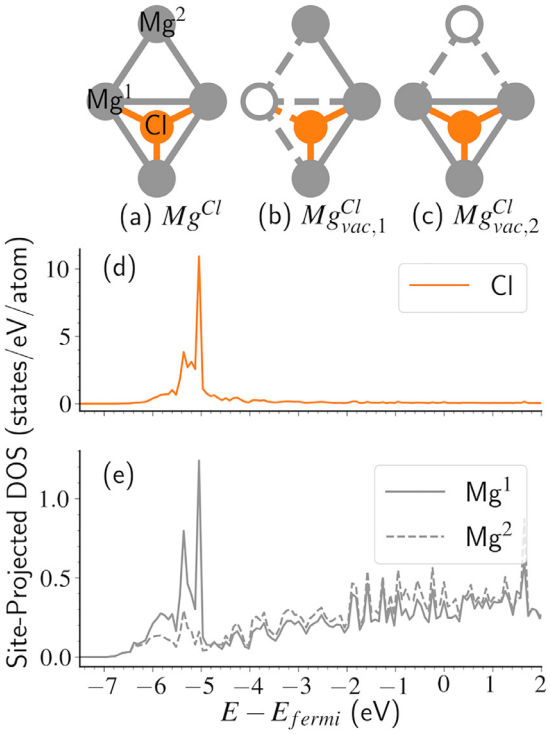

Fig. 4. (a) First ML of Mg atoms of Mg^{Cl} slab with Cl adsorbate at $\mathbf{F}_{Mg}$; orange dot is Cl adsorbate whose site-projected DOS is shown in (d); two types of Mg atoms are labelled as Mg^1, Mg^2, whose site-projected DOS is shown in (e); the grey lines are the metallic Mg-Mg bonds and orange lines are Mg-Cl bonds. (b)(c) two types of configuration of Mg^{Cl}_{vac} labelled as $Mg^{Cl}_{vac,1}$ and $Mg^{Cl}_{vac,2}$, corresponding the slab with removal of Mg^1 and Mg^2 respectively and it turns out that configuration in (c) is more energetic favoured and used in the determination of local electrode potential shift; the grey rings are Mg vacancies and the dashed lines are the broken bonds.

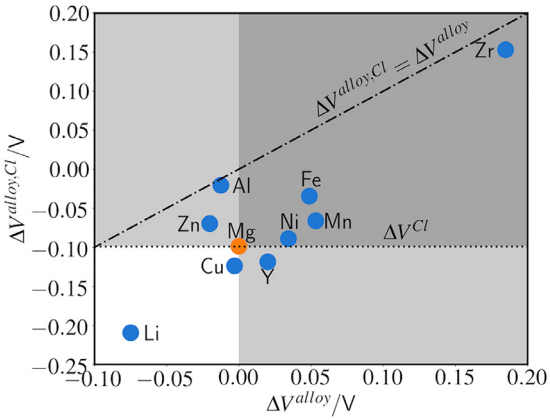

Fig. 5. Electrode potential shift on Mg (0001) introduced by surface solute atoms, ΔV^{alloy} vs. that by both surface solute atoms and Cl adsorbates, $\Delta V^{alloy,\,Cl}$.

Mg atoms are less compared to those before Cl adsorption, so that the metallic bonding between Mg atoms (grey lines in Fig. 4 (a)) appears be weakened, and only metallic bonds need to be broken to remove Mg^2 from surface as shown in Figure. 4 (c), and less energy is required to remove Mg^2 atom from surface after Cl adsorption consequently. Namely, Cl adsorbate destabilizes the Mg atom at surface.

3.2.2. Local electrode potential shift introduced by alloying

The local electrode potential shifts introduced by alloying with respect to pure clean Mg surface, ΔV^{alloy}, are displayed in Fig. 5. Positive

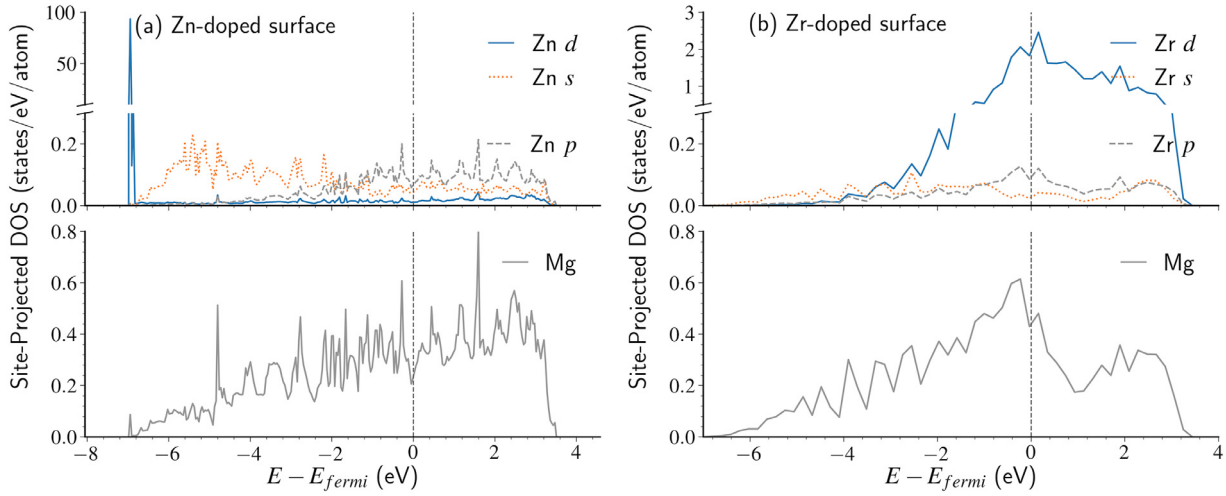

Fig. 6. (a) Site-projected DOS of Zn and Mg atoms at 25% Zn-doped surface. (b) Site-projected DOS of Zr and Mg atoms at 25% Zr-doped surface. Orbital projected DOS are also shown for Zn and Zr.

ΔV^{alloy} implies that the dopants stabilize the Mg atoms on the surface. It can be seen from Fig. 5 that dopants considered here with positive ΔV^{alloy} are all *d*-block elements. It is reported that the addition of *d*-block solute atoms results in higher bulk modulus of Mg matrix than *s* and *p*-block atoms [55], and a hybridization of *d* orbits of solute elements with the *s* and *p* orbits of Mg will enhance the bonding between solute atoms and Mg [56], which is also observed in our study for *d*-block elements.

Fig. 6 illustrates the projected DOS on the atoms of the Zn-doped and Zr-doped Mg surface respectively. The *d* orbits of Zr hybridizes with the orbits of Mg from ~4 eV below Fermi level to Fermi level, which implies a strong bonding between Zr and Mg and thus higher energy is necessary to remove the Mg atoms from the surface. In other words, the addition of Zr into Mg will stabilize the Mg atoms at surface and cause a positive local electrode shift. Although Zn also has *d*-electrons, they are highly localized below Fermi level at −7 eV as shown in Fig. 6 (a), which indicating little interaction between with the 3*s* or 3*p* orbits of Mg and *d* orbits of Zn. And the weak bonding between Zn and Mg leads to a negative electrode potential shift.

To further investigate the orbital in hybridization of Mg electrons with *d* electrons of *d*-block elements, we calculated the orbital energies of isolated *d*-block atoms of interests here with respect to vacuum. The closer of *d* orbital energy of dopant is to Fermi level of Mg slab, the greater the overlap is between the *d*-orbits of dopants and electron orbits Mg, and stronger hybridization is between the electrons on the orbits. By setting the vacuum level as zero, the Fermi level of Mg in the slab with respect to vacuum is just negative work function, −Φ. The order of orbital energies of all the *d*-block dopants considered here from high to low is: Y > −Φ > Zr > Mn > Fe > Ni > Cu > Zn. It agrees well as the local electrode potential order as shown in Fig. 5: Zr > Mn > Fe > Ni > Y > (pure Mg) > Cu > Zn, as closer energy levels lead to stronger hybridization. The exception of Y is believed to be caused by the fact that Y has only 1 *d* electron making the hybridization less strong.

3.2.3. Local electrode potential shift by both alloying and Cl adsorption

As mentioned, the Cl adsorption calculation is necessary to determine the most stable configuration of $Mg^{alloy,\ Cl}$ and $Mg_{vac}^{alloy,Cl}$ in Eq. (2) to calculate the electrode potential shift with regard to pure Mg surface. The most stable adsorption site and the corresponding energy, E_{ads}^{Cl} is shown in Table 2 and E_{ads}^{Cl} on all sites are listed in Table S1. As shown in Table 2, the surface dopants will stabilize the Cl adsorbate on the surface given by more negative Cl adsorption energy than that on pure Mg. The detailed discussion on Cl adsorption energy difference is in Figure.S1.

Local electrode potential shift by both alloying and Cl adsorption, $\Delta V^{alloy,\ Cl}$, is demonstrated in Fig. 5, along with that introduced only by alloying, ΔV^{alloy}. If $\Delta V^{alloy,\ Cl}$ is greater than the local potential introduced by Cl adsorbate, ΔV^{Cl}, Mg atoms on the corresponding alloyed surface with Cl adsorbate is more stable than those on pure Mg surface with Cl adsorbate.

It can be seen from Fig. 6 that all the elements lies below the line for $\Delta V^{alloy,Cl} = \Delta V^{alloy}$, which means the adsorption of Cl will shift down the electrode potential not only for pure Mg surface but all doped surfaces as well. Because Cl is much more electronegative than all the metals considered, it will lead to highly localized electrons way below Fermi level, which weakens the bonding between Mg and solute metals. This decrease in electrode potential of alloyed surface due to Cl adsorbate indicates the debilitating of the influence of doping elements in Cl ions aqueous. For example, it is found that for Y, $\Delta V^{alloy} > 0$, but $\Delta V^{alloy,\ Cl} < \Delta V^{Cl}$. Namely, the local electrode potential of Y-doped surface is higher that of pure Mg surface, whereas the presence of Cl makes the local electrode potential of Y-dope surface more negative than that of Mg surface with Cl adsorbate. From this prospective of view, solute Y atoms will beneficial in environments without Cl ions but less beneficial with Cl ions, which is consistent with experimental findings [57]. Nevertheless, positive correlation is still obvious between $\Delta V^{alloy,\ Cl}$ and ΔV^{alloy}, which proves that the bonds between Mg and dopants are still of importance. $\Delta V^{alloy,\ Cl}$ for Zr are still positive, which implies positive shift introduced by Zr wins over the negative shift introduced by Cl adsorbates. This remarkable positive shift in electrode potential regardless of the existence of Cl adsorbates provides theoretical evidence that Zr can stabilize the Mg at surface, delaying the localized corrosion and reducing the rate of anodic dissolution, which is experimentally indicated by Song and StJohn [13].

3.3. Summary of the influence of alloying elements and Cl adsorption on the work function and local electrode potential shift of Mg (0001)

Considering the solubility of alloying elements in Mg, 25% surface-doped rate might be closer to real situation and the corrosion behavior in the environment where Cl ions exist is of more interest. The influence of solute atoms on the work function (25% doping rate) and local electrode potential shift on Mg (0001) surface, is shown in Fig. 7. Elements in Region I and II (Al, Zn, Mn) will increase the barrier for charge transfer and stabilize surface Mg atoms, potential in depressing the anodic reaction, which actually consistent with prior experiments [58]. Elements in Region III (Cu, Li, Y) will decrease the barrier for charge transfer and destabilize surface Mg atoms, accelerating the anodic reaction. And in

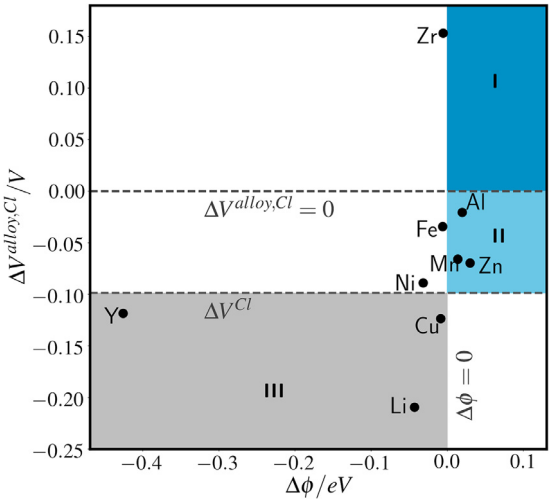

Fig. 7. Influence of solute elements on the work function change (25% doped surface) and local electrode potential shift on Mg (0001) introduced by both alloying atoms and Cl adsorbates. Region I: $\Delta\phi>0$, $\Delta V^{alloy,\ Cl}>0$; Region II: $\Delta\phi>0$, $\Delta V^{Cl}<\Delta V^{alloy,\ Cl}<0$; Region III: $\Delta\phi<0$, $\Delta V^{alloy,\ Cl}<\Delta V^{Cl}$.

remaining region (Zr, Fe, Ni), there is a compromise between the stability of charge and surface Mg atoms.

Albeit located in Region II, Zr can greatly and positively shift the local electrode potential and the decrease in work function introduced by Zr is nominal. So Zr atoms at surface should be able to depress the anodic dissolution by stabilizing the surface Mg atoms while its influence on charge transfer is trivial. On the other hand, although Ni and Fe will lead to positive shift in the local electrode potential according to our results, they can be notorious trace impurities as cathodes in Mg alloys considering their limited solubility in Mg, especially Fe. Whereas the anodic reaction of most Mg-Li alloys is reported to be accelerated [58,59] as predicted in our work, Xu et al.found in a specific Mg–Li alloy with bcc matrix and self-healing films that the anodic reaction can be much depressed [16]. In our model and simplification, we focus on the impact of alloy elements on the thermodynamic stability of electrons and Mg atoms on the surface of Mg hcp matrix. Although influence of alloying elements on other mechanisms such as passivation and structural difference is not included in our work, our model can serve as base to give a more comprehensive explanation on the influence of alloy elements on the corrosion behavior of Mg alloys.

4. Conclusions

By conducting first-principles calculations, we evaluated the influence of Cl adsorbates and solute atoms (Li, Y, Zr, Al, Mn, Fe, Cu and Ni) at surface on the anodic behavior of Mg matrix based on their influence on work function and local electrode potential. At 25% surface-doping rate, the change in work function introduced by aforementioned elements is less than 0.1 eV except Y. Their impact in work function indicates that only Y will greatly decrease the barrier for charge transfer while the influence of the remaining elements here on charge transfer is negligible at 25% surface-doping rate. Local electrode potential shift introduced by solute atoms and Cl adsorbates depends on their bonds with Mg atoms as well as the bonds between dopants and Cl. Cl adsorption will destabilize the Mg atoms on the surface by weakening the bonding between the metallic atoms on the surface. Those metallic dopants which could strongly bonding with Mg atoms on the surface, such as Zr, are likely to give rise to positive local electrode potential shift. It seems that *d*-block elements whose *d* electrons can hybridize strongly with the 3*s* and 3*p* electrons of Mg have the potential in stabilizing the Mg atoms on the surface.

Acknowledgments

H.Zhu thanks the start-up funding from Shanghai Jiao Tong University and the computational resources from Shanghai Jiao Tong University Super Computer Center.

Supplementary material

Supplementary material associated with this article can be found, in the online version, at doi:10.1016/j.susc.2018.02.002.

References

[1] B. Mordike, T. Ebert, Magnesium: properties applications potential, Mater. Sci. Eng. 302 (1) (2001) 37–45.
[2] K.U. Kainer, P. Bala Srinivasan, C. Blawert, W. Dietzel, Corrosion of magnesium and its alloys, Shreir's Corrosion 51 (8) (2010) 2011–2041.
[3] M.K. Kulekci, Magnesium and its alloys applications in automotive industry, Int. J. Adv. Manuf. Technol. 39 (9–10) (2008) 851–865.
[4] G. Song, A. Atrens, Understanding magnesium corrosiona framework for improved alloy performance, Adv. Eng. Mater. 5 (12) (2003) 837–858.
[5] G. Song, A. Atrens, D. St John, X. Wu, J. Nairn, The anodic dissolution of magnesium in chloride and sulphate solutions, Corros. Sci. 39 (10–11) (1997) 1981–2004.
[6] G.L. Song, A. Atrens, Corrosion mechanisms of magnesium alloys, Adv. Eng. Mater. 1 (1) (1999) 11–33.
[7] E. Ghali, W. Dietzel, K.-U. Kainer, General and localized corrosion of magnesium alloys: a critical review, J. Mater. Eng. Perform. 13 (1) (2004) 7–23.
[8] F. Cao, G.-L. Song, A. Atrens, Corrosion and passivation of magnesium alloys, Corros. Sci. 111 (2016) 835–845.
[9] A. Samaniego, K. Gusieva, I. Llorente, S. Feliu, N. Birbilis, Exploring the possibility of protective surface oxides upon Mg alloy Az31 via lutetium additions, Corros. Sci. 89 (2014) 101–110.
[10] M. Liu, P. Schmutz, P.J. Uggowitzer, G. Song, A. Atrens, The influence of yttrium (Y) on the corrosion of Mg–Y binary alloys, Corros. Sci. 52 (11) (2010) 3687–3701.
[11] F. Cao, Z. Shi, G.-L. Song, M. Liu, A. Atrens, Corrosion behaviour in salt spray and in 3.5% NaCl solution saturated with Mg (oh) 2 of as-cast and solution heat-treated binary Mg–x alloys: x= mn, sn, ca, zn, al, zr, si, sr, Corros. Sci. 76 (2013) 60–97.
[12] Z. Shi, F. Cao, G.-L. Song, M. Liu, A. Atrens, Corrosion behaviour in salt spray and in 3.5% nacl solution saturated with Mg (oh) 2 of as-cast and solution heat-treated binary Mg–re alloys: re= ce, la, nd, y, gd, Corros. Sci. 76 (2013) 98–118.
[13] G. Song, D. StJohn, The effect of zirconium grain refinement on the corrosion behaviour of magnesium-rare earth alloy mez, J. Light Met. 2 (1) (2002) 1–16.
[14] N. Birbilis, G. Williams, K. Gusieva, A. Samaniego, M. Gibson, H. McMurray, Poisoning the corrosion of magnesium, Electrochem commun 34 (2013) 295–298.
[15] R. Liu, M. Hurley, A. Kvryan, G. Williams, J. Scully, N. Birbilis, Controlling the corrosion and cathodic activation of magnesium via microalloying additions of ge, Sci. Rep. 6 (2016) 28747.
[16] W. Xu, N. Birbilis, G. Sha, Y. Wang, J.E. Daniels, Y. Xiao, M. Ferry, A high-specific-strength and corrosion-resistant magnesium alloy, Nat. Mater. 14 (12) (2015) 1229–1235.
[17] C.D. Taylor, A first-principles surface reaction kinetic model for hydrogen evolution under cathodic and anodic conditions on magnesium, J. Electrochem. Soc. 163 (9) (2016) C602–C608.
[18] O.I. Velikokhatnyi, P.N. Kumta, First-principles studies on alloying and simplified thermodynamic aqueous chemical stability of calcium-, zinc-, aluminum-, yttrium-and iron-doped magnesium alloys, Acta Biomater. 6 (5) (2010) 1698–1704.
[19] M. Chen, X.-B. Yang, J. Cui, J.-J. Tang, L.-Y. Gan, M. Zhu, Y.-J. Zhao, Stability of transition metals on Mg (0001) surfaces and their effects on hydrogen adsorption, Int. J. Hydrogen Energy 37 (1) (2012) 309–317.
[20] E. Casey, R. Bergeron, G. Nagy, On the mechanism of dissolution of magnesium in aqueous magnesium chloride solutions: part ii, Can. J. Chem. 40 (3) (1962) 463–479.
[21] J. Światowska, P. Volovitch, K. Ogle, The anodic dissolution of Mg in NaCl and na 2 so 4 electrolytes by atomic emission spectroelectrochemistry, Corros. Sci. 52 (7) (2010) 2372–2378.
[22] N. Lang, W. Kohn, Theory of metal surfaces: work function, Phys. Rev. B 3 (4) (1971) 1215.
[23] W. Li, D. Li, Variations of work function and corrosion behaviors of deformed copper surfaces, Appl. Surf. Sci. 240 (1) (2005) 388–395.
[24] X. Huang, H. Lu, D. Li, Understanding the corrosion behavior of isomorphous Cu-Ni alloy from its electron work function, Mater. Chem. Phys. 173 (2016) 238–245.
[25] J.O. Bockris, S.U. Khan, Surface Electrochemistry: A Molecular Level Approach, Springer Science & Business Media, 2013.
[26] S. Mosleh-Shirazi, G. Hua, F. Akhlaghi, X. Yan, D. Li, Interfacial valence electron localization and the corrosion resistance of Al-sic nanocomposite, Sci. Rep. 5 (2015).
[27] Q. Li, H. Lu, J. Cui, M. An, D.D. Li, Understanding the low corrosion potential and high corrosion resistance of nano-zinc electrodeposit based on electron work function and interfacial potential difference, RSC Adv. 6 (100) (2016) 97606–97612.
[28] K. Yasuda, A. Taniguchi, T. Akita, T. Ioroi, Z. Siroma, Platinum dissolution and deposition in the polymer electrolyte membrane of a pem fuel cell as studied by potential cycling, PCCP 8 (6) (2006) 746–752.
[29] R. Ramprasad, P. von Allmen, L. Fonseca, Contributions to the work function: a density-functional study of adsorbates at graphene ribbon edges, Phys. Rev. B 60 (8) (1999) 6023.

[30] P. Khomyakov, G. Giovannetti, P. Rusu, G.v. Brocks, J. Van den Brink, P. Kelly, First-principles study of the interaction and charge transfer between graphene and metals, Phys. Rev. B 79 (19) (2009) 195425.
[31] H. Zhu, M. Aindow, R. Ramprasad, Stability and work function of tic x n 1- x alloy surfaces: density functional theory calculations, Phys. Rev. B 80 (20) (2009) 201406.
[32] S.-T. Cheng, M. Todorova, C. Freysoldt, J. Neugebauer, Negatively charged ions on Mg (0001) surfaces: appearance and origin of attractive adsorbate-adsorbate interactions, Phys. Rev. Lett. 113 (13) (2014) 136102.
[33] J. Greeley, J.K. Nørskov, Electrochemical dissolution of surface alloys in acids: thermodynamic trends from first-principles calculations, Electrochim. Acta 52 (19) (2007) 5829–5836.
[34] Y. Ma, P.B. Balbuena, Surface properties and dissolution trends of Pt3m alloys in the presence of adsorbates, J. Phys. Chem. C 112 (37) (2008) 14520–14528.
[35] C. Han, C. Zhang, X. Liu, S. Zhuang, H. Huang, P. Han, X. Wu, Dft study of the effects of interstitial impurities on the resistance of Cr-doped γ-fe (111) surface dissolution corrosion, J. Mol. Model. 21 (8) (2015) 206.
[36] G. Kresse, J. Hafner, Ab initio molecular dynamics for liquid metals, Phys. Rev. B 47 (1) (1993) 558–561, doi:10.1103/PhysRevB.47.558.
[37] J.P. Perdew, K. Burke, M. Ernzerhof, Generalized gradient approximation made simple, Phys. Rev. Lett. 77 (18) (1996) 3865.
[38] P.E. Blöchl, Projector augmented-wave method, Phys. Rev. B 50 (24) (1994) 17953.
[39] E. Owen, L. Pickup, I. Roberts, et al., Lattice constants of five elements possessing hexagonal structure, Zeitschrift für Kristallographie-Crystalline Materials 91 (1–6) (1935) 70–76.
[40] M. Methfessel, A. Paxton, High-precision sampling for Brillouin-zone integration in metals, Phys. Rev. B 40 (6) (1989) 3616.
[41] P.E. Blöchl, O. Jepsen, O.K. Andersen, Improved tetrahedron method for brillouin–zone integrations, Phys. Rev. B 49 (23) (1994) 16223.
[42] R. Tran, Z. Xu, D.W. Balachandran Radhakrishnan, W. Sun, K.A. Persson, S.P. Ong, Surface energies of elemental crystals, Sci. Data 3 (2016).
[43] P. Zhou, C. Zhou, H.R. Gong, Chlorine adsorption on Mg, Ca, and MgCa surfaces, Mater. Sci. Eng., C 33 (7) (2013) 3826–3831.
[44] H.B. Michaelson, The work function of the elements and its periodicity, J. Appl. Phys. 48 (11) (1977) 4729–4733.
[45] E. Wachowicz, A. Kiejna, Bulk and surface properties of hexagonal-close-packed be and Mg, J. Phys. 13 (48) (2001) 10767.
[46] F. Mansfeld, Y. Wang, Corrosion protection of high copper aluminium alloys by surface modification, Br. Corros. J. 29 (3) (1994) 194–200.
[47] M. Gatalo, Positive effect of surface doping with au on the stability of Pt-based electrocatalysts, ACS Catal. 6 (3) (2016) 1630–1634.
[48] T. Cain, S. Madden, N. Birbilis, J. Scully, Evidence of the enrichment of transition metal elements on corroding magnesium surfaces using rutherford backscattering spectrometry, J. Electrochem. Soc. 162 (6) (2015) C228–C237.
[49] R. Huggins, Advanced Batteries: Materials Science Aspects, Springer Science & Business Media, 2008.
[50] A. Atrens, W. Dietzel, The negative difference effect and unipositive Mg +, Adv. Eng. Mater. 9 (4) (2007) 292.
[51] T. Leung, C. Kao, W. Su, Y. Feng, C. Chan, Relationship between surface dipole, work function and charge transfer: some exceptions to an established rule, Physical Review B 68 (19) (2003) 195408.
[52] E. Wigner, J. Bardeen, Theory of the work functions of monovalent metals, Phys. Rev. 48 (1) (1935) 84.
[53] J.C. Slater, Atomic radii in crystals, J. Chem. Phys. 41 (10) (1964) 3199–3204.
[54] P.M. Rice, W.D. Kingery, H. Bowen, D.R. Uhlmann, G.Y. Onoda, L.L. Hench, J.B. Wachtman, W.R. Cannon, M.J. Matthewson, Physical ceramics: principles for ceramic science and engineering (1997).
[55] S. Ganeshan, S. Shang, H. Zhang, Y. Wang, M. Mantina, Z. Liu, Elastic constants of binary Mg compounds from first-principles calculations, Intermetallics 17 (5) (2009) 313–318.
[56] K. Chen, K.P. Boyle, Alloy solid solution strengthening of Mg alloys: valence effect, Physica Status Solidi (b) 249 (11) (2012) 2089–2095.
[57] A. Sudholz, K. Gusieva, X. Chen, B. Muddle, M. Gibson, N. Birbilis, Electrochemical behaviour and corrosion of Mg–y alloys, Corros Sci 53 (6) (2011) 2277–2282.
[58] M. Esmaily, J. Svensson, S. Fajardo, N. Birbilis, G. Frankel, S. Virtanen, R. Arrabal, S. Thomas, L. Johansson, Fundamentals and advances in magnesium alloy corrosion, Prog. Mater. Sci. (2017).
[59] Y. Song, D. Shan, R. Chen, E.-H. Han, Corrosion characterization of Mg–8li alloy in NaCl solution, Corros. Sci. 51 (5) (2009) 1087–1094.